An analytical model for the scattering of guided waves by partly through-thickness cavities with irregular shapes in 3D

Ludovic Moreau, Mihaï Caleap, Alexander Velichko, Paul D. Wilcox

ACOUSTICS 2012

An analytical model for the scattering of guided waves by partly through-thickness cavities with irregular shapes in 3D

L. Moreau[a], M. Caleap[b], A. Velichko[b] and P.D. Wilcox[b]

[a]UPMC CNRS LIP, 15 rue de l'école de médecine, 75006 Paris, France
[b]University of Bristol, Queen's Building, University Walk, BS81TR Bristol, UK
ludovic.moreau@upmc.fr

Abstract

This paper investigates the three-dimensional (3D) scattering of guided waves by a partly through-thickness, flat-bottomed cavity with an irregular shape, in an isotropic plate. A comparison is made between results from an analytical model recently developed and those from an efficient finite element model optimized for guided wave problems. In the analytical solution, both the scattered field and the standing field in the thinner plate beneath the cavity are decomposed on the basis of Lamb and SH waves, by including propagating and evanescent modes. The amplitude of the modes is calculated after writing the nullity of the total stress at the boundary of the cavity, and the continuity of the stress and displacement vectors under the cavity. In the boundary conditions, the functions depend on the through-thickness coordinate, z, and on the angular coordinate, θ, because the cavity is not circular. This is dealt with by projecting the z-dependent functions onto the basis of the guided waves displacements vectors, and by expanding the θ-dependent functions in Fourier series. Example results are presented for the scattering of the S_0 mode by an elliptical cavity and a cavity with an arbitrary shape.

1 Introduction

Modelling the interaction of acoustic waves with scatterers is a major preoccupation in many areas, such as medicine or Non-Destructive Evaluation (NDE). Due to specific difficulties linked to the scattering of guided waves, numerical approaches often prevail in the NDE area [1]. Analytical solutions have been found in 2D for a limited number of cases only, for which the geometry of the cavity remains simple. In 3D, finding such solutions is even more complex, and semi-analytical solutions exist only for partly-through-thickness cavities with a circular shape [2], or through-thickness cavities with an irregular shape [3].

In this context, the finite element (FE) or boundary element (BE) methods have become a common way to model Lamb wave scattering problems. However, a full 3D investigation with numerical methods is highly computationally expensive. Even on powerful machines, computational times remain of the order of several hours for one particular incident wave field. Analytical or semi-analytical solutions to such problems are therefore desirable. They provide independent validation of numerical methods and enable rapid simulations of scattering from large populations of different scatterers. They also enable the relative contributions of different modes (e.g. propagating or non-propagating) to be examined to provide insight into the physics of the scattering process.

This paper introduces an analytical solution for the scattering of ultrasonic guided waves by flat-bottomed cavities with an arbitrary shape, in a flat, isotropic plate. It is a generalization of our previous work, which was limited to through-thickness cavities [3]. The partly through-thickness case is more complex, because in addition to the incident and scattered fields, the acoustic field also contains a standing field under the cavity.

The problem is solved in a cylindrical coordinate system r, θ, z, where z is normal to the plate surface. The incident, scattered and standing fields are expanded in the possible propagating and non-propagating Lamb and shear-horizontal modes, the expansion coefficients of which must be found. This is made difficult due to the dependency on z and θ of the functions in the boundary conditions. One solution to this problem, consist of projecting the stress and displacement vectors onto the displacements vectors of the guided wave modes, which allows the transormation of the z- dependent functions into coefficients. Then the θ-dependent functions are expanded into Fourier series. It is presented in secion 2. This new projection method is more stable and converges faster than the projection introduced in [2], which is not stable enough for cavities with a non-circular shape.

Two types of examples are presented for validation purpose in section 4. In the first example, the scattering of S_0, A_0 and SH_0 by an elliptical cavity is studied. Different depths and aspect ratios are considered for the cavity. In the second example, the scattering matrix [4] of an irregular cavity is calculated when the S_0 Lamb wave mode is incident. Validations of the results are performed by comparing the solution with results from a FE model, and by computing the energy balance of the scattering problems.

2 Theory

2.1 Notation

Consider a partly through-thickness, prismatic cavity in an infinite plate made of a homogeneous, isotropic material. The plate thickness is $2h$ and the thickness under the cavity is $2b$. We assume the surfaces of both the plate and the cavity to be traction free. When an incident acoustic field hits the cavity, a scattered field is generated in the plate, but part of the incident energy is also converted into a standing field of guided waves under the cavity. Let (O, x, y, z) and (O', x', y', z') be the Cartesian coordinate systems in the plate and under the cavity, respectively, where z and z' are normal to the plane of the plate (figure 1). The origin O and O' of the coordinate systems are located as shown in figure 1. To express the acoustic fields resulting from the scattering of a guided wave by the cavity, we introduce (O, r, θ, z), a cylindrical coordinate system. The polar coordinates (r, θ) are related to the Cartesian coordinates (x, y) such that $r^2 = x^2 + y^2$ and $\cos\theta = x/r$ (figure 1).

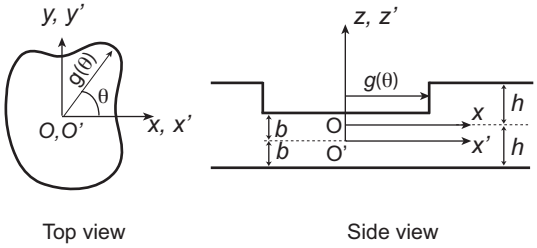

Figure 1: Definition of the coordinates system for the scattering problem

The displacement field produced by a scattered Lamb wave mode of order n (symmetric or antisymmetric) propagating in the plate of thickness $2h$ can be expressed as [5]:

$$\mathbf{U}^{n,>} = \begin{bmatrix} U_r^{n,>}(r,\theta,z) \\ U_\theta^{n,>}(r,\theta,z) \\ U_z^{n,>}(r,\theta,z) \end{bmatrix} = \begin{bmatrix} \frac{1}{k} V_n^h(z) \frac{\partial \Phi^>}{\partial r}(r,\theta) \\ \frac{1}{k} V_n^h(z) \frac{1}{r} \frac{\partial \Phi^>}{\partial \theta}(r,\theta) \\ W_n^h(z) \Phi^>(r,\theta) \end{bmatrix}. \quad (1)$$

For SH waves, the displacement field is given by [5]:

$$\mathbf{U}^{n,>} = \begin{bmatrix} U_r^{n,>}(r,\theta,z) \\ U_\theta^{n,>}(r,\theta,z) \\ U_z^{n,>}(r,\theta,z) \end{bmatrix} = \begin{bmatrix} \frac{1}{k} V_n^h(z) \frac{1}{r} \frac{\partial \Psi^>}{\partial \theta}(r,\theta) \\ -\frac{1}{k} V_n^h(z) \frac{\partial \Psi^>}{\partial r}(r,\theta) \\ 0 \end{bmatrix}. \quad (2)$$

In the above expressions, V_n^h and W_n^h are the through-thickness displacement fields of Lamb or SH modes. They can be found for example in ref. [5]. The displacement field of standing guided waves beneath the cavity is expressed in a similar way, by replacing $>$ by $<$, h by b, and z by $z\prime$ in the above equations. The scalar potentials Φ and Ψ define the expansion functions for the wave fields of Lamb and SH modes, respectively. Their expressions can be found in ref. [6].

The stress field for the scattered ($\boldsymbol{\sigma}^>$), standing ($\boldsymbol{\sigma}^<$), and incident ($\boldsymbol{\sigma}^{in}$) waves is calculated from Eqs. (1) and (2) using Hooke's law in polar coordinates.

2.2 Boundary conditions associated with the problem

In the following, we assume that the shape of the cavity is defined by $r = g(\theta)$, where g is a function that must be at least once differentiable with respect to the variable θ, so that the outward normal to the cavity, $\mathbf{n}$, can be calculated. When a guided wave is incident on the cavity, the scattered, standing and incident fields must satisfy the following boundary conditions:

$$\begin{cases} \boldsymbol{\sigma}^> \mathbf{n} = -\boldsymbol{\sigma}^{in} \mathbf{n}, & -h + 2b < z < h, \quad r = g(\theta) \\ \left[\boldsymbol{\sigma}^> - \boldsymbol{\sigma}^<\right] \mathbf{n} = -\boldsymbol{\sigma}^{in} \mathbf{n}, & -h < z < -h + 2b, \quad r = g(\theta), \\ \mathbf{U}^> - \mathbf{U}^< = -\mathbf{U}^{in}, & -h < z < -h + 2b, \quad r = g(\theta). \end{cases} \quad (3)$$

where, the outward normal to the scatterer, $\mathbf{n}$, is given by:

$$\mathbf{n}(\theta) = \begin{pmatrix} n_r(\theta) \\ n_\theta(\theta) \\ 0 \end{pmatrix} = \frac{1}{\sqrt{g(\theta)^2 + g'(\theta)^2}} \begin{pmatrix} g(\theta) \\ -g'(\theta) \\ 0 \end{pmatrix}. \quad (4)$$

The functions in the boundary conditions depend on the z coordinate, due to the mode shapes, and on the θ coordinate, due to the shape of the cavity. Although this problem seems similar to the case of the through-thickness cavity [3], in practice it must be solved with a different approach. When solving the through-thickness cavity case, the dependency on the z coordinate was dealt with by using a projection method similar to that proposed in ref. [2], where the author solves the case of a cavity with a circular shape. There is therefore no dependency on θ in the boundary conditions. In [2], the z-dependency is dealt with by projecting the boundary conditions onto a set of orthogonal functions of z. A different basis of cosine functions is used for the displacement and stress boundary conditions:

- the 3 components of the vector of the stress boundary condition are multiplied by $\cos(\frac{n\pi z}{2h})$ and integrated over the thickness of the plate ($2h$),

- the 3 components of the vector of the displacement boundary conditions are multiplied by $\cos(\frac{n\pi z}{2b})$ and integrated over the thickness underneath the cavity ($2b$)

In this approach, each different value of n in the projection functions allows the creation of 3 new equations (3 for the stresses or 3 for the displacements). This requires that the same number of symmetric Lamb modes, antisymmetric Lamb modes, and SH modes is included into the scattered and standing fields, so that the system contains as many equations as unknowns. Consequently, some evanescent modes of a given type may be included in the scattered or standing fields, even though they are much more attenuated than modes of another type which are not included. Indeed, the influence of the non-propagating modes on the acoustic field depends on the imaginary part of their wavenumber: the higher this imaginary part, the more attenuated the mode, and then the less contribution to the acoustic field. Including a mode of a given type (e.g. a symmetric Lamb mode) that is highly attenuated rather than a mode of another type (e.g. an antisymmetric Lamb mode or SH mode) which contribution to the acoustic field is greater can cause instabilities in the solution. This is because highly attenuated modes worsen the conditioning of the final system to be inverted.

Although this method is stable enough for a circular cavity, a more stable one is required, when the shape of the cavity is not circular, because in that case more instabilities are created due to the dependency on θ in the boundary conditions. However, the approach to the dependency on θ suggested in ref. [3] (i.e. expanding the θ-dependent function into Fourier series) is stable enough and will be used here as well.

2.3 Projection of the boundary conditions

We suggest a different projection method, in which it is possible to select the modes to be included in the summations. In our approach to the boundary conditions, instead of using a scalar projection function for each component of the displacement and stress vectors, we use the displacement vector of the modes. The stress boundary condition is projected on the displacement of the modes in the scattered field,

$$\mathbf{U}_{p'}^{n_1',>} = \mathrm{conj} \begin{bmatrix} U_{p',r}^{n_1',>}(a,\theta,z) \\ U_{p',\theta}^{n_1',>}(a,\theta,z) \\ U_{p',z}^{n_1',>}(a,\theta,z) \end{bmatrix} \mathrm{e}^{-\mathrm{i}p'\theta}. \quad (5)$$

With this choice of projection vector, the projection of the stress boundary condition is similar to the orthogonality relationship that naturally exists between the stress and displacement mode shapes of different guided wave modes. This will create more zeros in the final system to be inverted. The displacement boundary condition is projected on the displacement of the modes in the standing field,

$$\mathbf{U}_{p'}^{n_2',<} = \mathrm{conj} \begin{bmatrix} U_{p',r}^{n_2',<}(a,\theta,z') \\ U_{p',\theta}^{n_2',<}(a,\theta,z') \\ U_{p',z}^{n_2',<}(a,\theta,z') \end{bmatrix} \mathrm{e}^{-\mathrm{i}p'\theta}. \quad (6)$$

Here the choice of this projection vector is for consistancy with the projection vectors for the stress boundary condition.

In these equations, conj denotes the complex conjugation, a is a constant set equal to the minimum radius of the cavity, and p' refers to the p'^{th} term of the Fourier order of the displacement [6]. n'_1 and n'_2 represent the indices of the modes used in the projection vectors for the stress and displacement boundary conditions, respectively.

After projection, the boundary conditions become:

$$\begin{aligned}\int_{-h}^{h}[\boldsymbol{\sigma}^{>}-\boldsymbol{\sigma}^{<}]\,\mathbf{n}\cdot\mathbf{U}_{p'}^{n'_1,>}\mathrm{e}^{-\mathrm{i}p'\theta}dz &= -\int_{-h}^{h}\boldsymbol{\sigma}^{in}\mathbf{n}\cdot\mathbf{U}_{p'}^{n'_1,>}\mathrm{e}^{-\mathrm{i}p'\theta}dz,\ \forall n'_1\in\mathbb{Z},\\ \int_{-b}^{b}[\mathbf{U}^{>}-\mathbf{U}^{<}]\cdot\mathbf{U}_{p'}^{n'_2,<}\mathrm{e}^{-\mathrm{i}p'\theta}dz &= -\int_{-b}^{b}\mathbf{U}^{in}\cdot\mathbf{U}_{p'}^{n'_2,<}\mathrm{e}^{-\mathrm{i}p'\theta}dz,\ \forall n'_2\in\mathbb{Z},\end{aligned} \tag{7}$$

where $\mathbb{Z}$ denotes the group of negative and positive integers. The dependency on z is now transformed into projection coefficients related to the mode shapes. They can be calculated numerically or by developing closed-form expression of the integrals.

Dealing with the dependency on θ requires a stable approach too. For this purpose, the θ-dependent functions are expanded into Fourier series. After some developments, one can write the system to invert in a matrix form

$$\mathbf{Aa} = \mathbf{b}, \tag{8}$$

where $\mathbf{A}$ is an infinite block matrix containing θ-dependent informations about the scattered and standing fields, $\mathbf{b}$ is an infinite vector containing informations relative to the incident field, and $\mathbf{a}$ is the unknown infinite vector containing the amplitudes of all modes. We refer the reader to ref. [6] for the full mathematical details of this method.

Note that the theory developed in this paper is based on the assumption that outgoing waves can be used to describe the scattered field at any point outside the scatterer, and in particular inside its circumscribed cylinder. This is known as the Rayleigh hypothesis [7], the validity of which is still an ongoing research topic. However, as explained in [3], expanding the acoustic fields into Fourier series allows a stable and accurate solution to be calculated, regardless of the validity of the Rayleigh hypothesis.

2.4 Numerical considerations

In order to solve the scattering problem a truncation must be made in the infinite summations over n_1, n_2, m, and p in Eq. (8). We define the following truncation numbers:

N_1, the number of modes ξ_n included in the modal decomposition of the scattered field;

N_2, the number of modes ξ_n included in the modal decomposition of the standing field;

M, the number of angular expansion coefficients a_m for all modes ξ_n;

P, the number of terms in the Fourier series decompositions.

Each of these truncation numbers must be subject to a convergence study prior to solving the problem.

The number of guided wave modes N_1 is mostly dependent on the frequency-thickness of the plate, while N_2 depends on the frequency-thickness under the cavity. The higher these products, the greater N_1 and N_2. Therefore, the rule of thumb indicated in ref. [2] seems appropriate:

$$N_2 \approx \frac{bN_1}{h} \tag{9}$$

The number of modes of each type (i.e. symmetric Lamb modes, antisymmetric Lamb modes and SH modes) to be included in the acoustic fields is determined after sorting all modes according to the increasing imaginary part of their wavenumber. Then the first N_1 modes (or N_2 in the standing field) are selected.

It was shown in ref. [3] that the other two truncation numbers, M and P, must be such that

$$2P+1 = 2M+1 = \max[Q, 2\pi D/\min(\lambda_n)], \tag{10}$$

where D is the largest dimension of the cavity, $\min(\lambda_n)$ is the smallest wavelength of the propagating modes, and Q is the number such that if $P \geqslant Q$, convergence is achieved in the Fourier series.

The number of unknowns of the scattering problem is then $(N_1+1)(2M+1)$ in the scattered field and $(N_2+1)(2M+1)$ in the standing field, e.g. $(2M+1)$ unknown expansion coefficients a_m for each of the modes. To determine these unknowns, we create the required number of equations by setting $n' = 0, 1, ..., N_1$ in the scattered field and $n' = 0, 1, ..., N_2$ in the standing field, and $p = 0, \pm1, ..., \pm M$. When the geometry of the scatterer contains tight curves, which is the case for example for an ellipse with a very small aspect ratio, the number of Fourier terms P increases.

3 Convergence and stability of the scalar and vectorial projection methods

In this section, the scalar and vectorial projection methods are compared in terms of convergence and stability. To this end, the scattering of the S_0 mode by a flat-bottom, circular hole in a steel plate of thickness 5 mm is studied at the frequency 200 kHz. The diameter of the cavity is equal to 26 mm, which is the wavelength of the incident mode at the considered frequency-thickness. The only geometrical parameter that varies is the depth of the hole.

The convergence of the solution is studied only in terms of the number of modes to be included in the standing and the scattered field, since the convergence parameter related to the angular order, M, is the same for both projection methods. In this study we determine the minimum numbers N_1 and N_2 required for the convergence of each method. These are shown in table 1, for different depths of the cavity. Compared to the scalar projection, the total number of modes $N_1 + N_2$ required by the vectorial projection is always inferior by 2 to 4 modes, which indicates faster convergence.

	b/h	0.9	0.8	0.7	0.6	0.5	0.4	0.3	0.2	⩽0.1
scalar projection method	N1	9	9	9	9	9	9	9	9	9
	N2	6	6	6	6	6	6	3	3	3
vectorial projection method	N1	7	7	7	7	7	7	7	7	7
	N2	6	6	5	5	4	4	3	3	3

Table 1: Comparison between the convergence parameters of the scalar and the vectorial projection method.

To study the stability of the two projection methods, the convergence numbers N_1 and N_2 are varied and the corresponding solution of the scattering problem is computed. These numbers take the following 3 sets of values: {9;6}, {12;6} and {15;9}. These values are imposed by the fact that for the scalar projection method, N_1 and N_2 have to be multiples of 3. Note that this is not the case for the vectorial projection method which allows any values to be chosen. However, for

the sake of the comparison, the values of N_1 and N_2 are chosen to be the same for both methods. It was observed that the scalar projection method leads to an unstable solution that diverges as soon as the convergence numbers are increased. On the other hand, the vectorial projection method shows a very stable behavior.

4 Examples

In this section we present two examples of scatterer geometries. Each type of geometry is validated by comparison with FE results, and by computing the energy balance.

4.1 Validation of the results

Because no other semi-analytical model exists for the scattering of ultrasonic guided waves in 3D, results obtained with the method described in section 2 are compared to results from the FE method. The FE model used for the simulations is based on the Huygens's principle to generate the incident wave and perform the modal decomposition of the scattered field. In this frequency-domain approach, reflections from the edges of the model are prevented by using a classical absorbing region that surround the area of interest. This model is presented in several references and will not be described further here. A detailed description can be found, for example, in ref. [8].

The far field amplitudes of the scattered modes are calculated from both the analytical model and the FE model, and compared for validation. Another way of checking the results of the models is to compute the energy balance of the total (incident+scattered) field. This can be achieved using the far field amplitude of the modes in the way described in ref. [8]. Although the energy balance is not a sufficient condition to prove that the solution is correct, it is a necessary condition that should be checked.

4.2 Scattering by elliptical cavities

In this section, the scattering of the S_0 mode by partly through-thickness elliptical cavities is investigated at a frequency-thickness of 500 kHz.mm, with the plate thickness equal to 5 mm. We denote by a_y and a_x the major and minor half axes of the ellipses, respectively. In the cases investigated here, the aspect ratio a_x/a_y of the ellipses is varied from 1/4 to 1, and so is the fractional depth of the cavity. Cases where the S_0, A_0 and SH_0 modes are incident on the cavity are presented. In every example, the largest dimension of the ellipse, $2a_y$, is set to be half the wavelength of the incident mode.

In this study, tests have shown that $N_1 = 10$ and N_2 set according to Eq. (9) allows the convergence of the solution. The value of the other truncation number, M, depends on the largest dimension of the ellipse relative to the mode with the smallest wavelength in the scattered field. The larger this ratio, the more terms are needed for the convergence of the Fourier series [3]. Moreover, the smaller the aspect ratio of the ellipse, the more terms are required in the Fourier series. Therefore, the convergence was investigated only for the case $a_x/a_y = 1/4$, in order to set M for all values of a_x/a_y greater than 1/4. It was found that $M = 11$ allows the convergence of the results.

Comparison with FE results is made only for the cases $a_x/a_y = 1$ and $a_x/a_y = 1/4$ when the depth of the cavity is half the plate thickness, and when the S_0 mode is incident at the angle θ_{in} equal to 0. This is presented in figure 2, which shows very good agreement between the two methods, although some minor differences can be noticed for the three modes. For further validation, the energy balance was calculated. For the analytical model, it is less than 2% when $a_x/a_y = 1/4$, and less than 1% when $a_x/a_y = 1$. For the FE model, the energy balance is less than 4% when $a_x/a_y = 1/4$, and less than 5% when $a_x/a_y = 1$. The energy balance is not as good for the FE model as for the analytical model. It is believed that this is linked to the efficiency of the absorbing region. Indeed, for 3D modelling, tests have shown that the absorbing region seems to be not as efficient for the antisymmetric modes as it is for symmetric or SH modes. This was pointed out in ref. [8], where minor differences were also discovered for the A_0 mode, for a circular, partly through-thickness cavity.

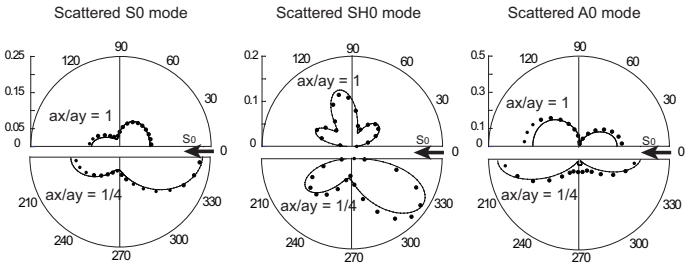

Figure 2: FE (line) and analytical (dots) predictions of the far-field amplitude of the scattered modes when the S_0 mode is incident on an elliptical cavity. Parameters: frequency-thickness = 500 kHz.mm, $b/h = 1/2$, and $a_x/a_y = 1$ (top half) or $a_x/a_y = 1/4$ (bottom half).

4.3 Scattering by an irregular cavity

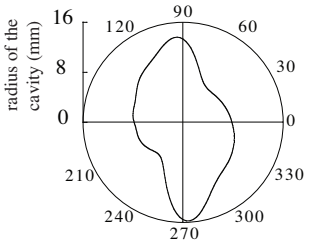

Figure 3: Shape of the irregular cavity (length is in mm)

In this section, we calculate the scattering matrix of an irregular cavity, the shape of which is plotted in figure 3. The corresponding function has been defined in a heuristic way, so that a cavity of random geometry is created for illustrative purpose. The function is therefore not given here. The convergence parameters for this study are such that $N_1 = 10$, $N_2 = 5$ and $M = 10$. The truncation numbers N_1 and N_2 are the same as in the previous study, when S_0 is incident. This was expected, as they depend only on the incident mode and the frequency-thickness product, but not on the geometry of the cavity, so long as it is flat-bottomed. The scattering matrix of a cavity is the far-field behaviour of the scattered waves for any combination of incident and scattered angles [4]. Considering all incident angles, the maximum error in the energy balance was 2% for the analytical model. The scattering matrices are calculated with 20 incident angles,

and are then interpolated in the Fourier domain for better resolution. They are represented in figure 4, which shows very good agreement for the S_0 and SH_0 modes. Some differences can be observed for the A_0 mode, once again due to the absorbing region. This is also revealed in the energy balance, which is not as good for the FE model (5%) as it is for the analytical model. Overall, agreement between the results calculated with both methods is very good, thus validating our model.

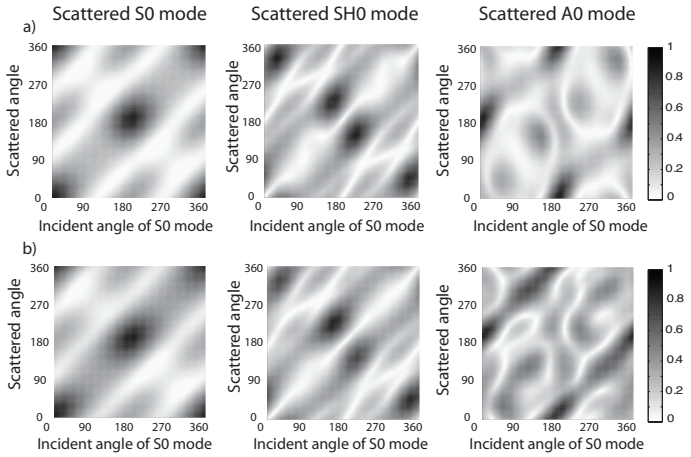

Figure 4: Scattering matrix of the irregular cavity calculated a) with the analytical method and b) with the FE method.

5 Conclusions

This paper has presented an analytical method to solve the scattering of guided waves by partly-through thickness, flat-bottomed cavities of arbitrary shape. The method was validated by comparison with the FE method for two types of examples, and by calculating the energy balance of the scattering problems. In the first type of example, the cavity has an elliptical shape, and results between the two methods showed very good agreement. Cases where either the S_0, A_0 or SH_0 mode is incident were presented for different depths of the elliptical cavity. In the second type of example, the complete scattering matrix of a cavity with an irregular shape was calculated, again showing very good agreement with the FE results.

This method is computationally very efficient because it offers an analytical alternative to numerical approaches such as FEM or BEM for guided wave scattering problems. From a practical point of view, it can be used in a Non-Destructive Evaluation context, for example as a first approximation to the modelling of scattering from corrosion patches.

References

[1] J. Meckerle, Finite-element modelling of non-destructive material evaluation, an addendum: a bibliography (1997-2003), *Modell. Simul. Mater. Sci. Eng.* 12(5), (2004) 799–834.

[2] T. Grahn, Lamb wave scattering from a circular partly through-thickness hole in a plate , *Wave Motion* 37(1), (2003) 63–80.

[3] L. Moreau, M. Caleap, A. Velichko and P. D. Wilcox Scattering of guided waves by through-thickness cavities with irregular shapes , *Wave Motion* 48(7) (2011) 586–602

[4] J. Zhang, B. Drinkwater, and P. Wilcox Defect characterization using an ultrasonic array to measure the scattering coefficient matrix, *IEEE Trans. Ultrason., Ferroelect., Freq. Contr.* 55(10), (2008) 2254–2265 .

[5] J. D. Achenbach and Y. Xu, Wave motion in an isotropic elastic layer generated by a time-harmonic point load of arbitrary direction, *J. Acoust. Soc. Am.* 106 (1), (1999) 83–90.

[6] L. Moreau, M. Caleap, A. Velichko and P. D. Wilcox Scattering of guided waves by flat-bottomed cavities with irregular shapes , *Wave Motion* 49(2), (2012) 375–387

[7] Lord Rayleigh, On the dynamical theory of gratings, *Proc. R. Soc. London Ser.* A 79, (1907) 399–416.

[8] A. Velichko and P. D. Wilcox, A generalized approach for efficient finite element modelling of elastodynamic scattering in two and three dimensions, *J. Acoust. Soc. Am.* 128(3), (2010) 1004–1014.